HiSST: 2nd International Conference on
High-Speed Vehicle Science Technology
11–15 September 2022, Bruges, Belgium

Temporary Fiber Bragg Grating Sensors for Static and Dynamic Strain Measurements in Hypersonic Wind Tunnels

L. Pollock[1], G. Wild[2]

Abstract

This paper reports on the results of a preliminary investigation into three different adhesive tapes – Washi acrylic masking, high-temperature fiberglass backed aluminum, and double-sided acrylic tissue - for temporarily bonding Fiber Bragg Gratings (FBGs) to a metallic substrate. The development and analysis of suitable temporary adhesives allows for rapid testing and conservation of expensive optical componentry in hypersonic wind tunnel tests. Tensile testing was undertaken wherein force and displacement values are recorded. A Thorlabs S5FC1005S Super Luminescent Diode (SLED) is used to illuminate the FBG following which a Photonetics WALICS Optical Spectrum Analyzer (OSA) is utilized to obtain the reflected optical spectrum. The shift in spectrum is analyzed using a Generalized Cross-Correlation (GCC) and compared to measured strain values to determine the sensitivity and linearity of the FBG response for each of the adhesives. It was found that all tapes resulted in low strain efficiencies but relatively linear responses.

Keywords: *Fiber Bragg Grating (FBG), adhesive, hypersonic, testing, metrology*

1. Introduction

Hypersonic vehicles (HSVs) have found a renewed interest in recent decades, primarily due to security concerns. Despite such investment, the extreme environments in which HSVs operate have contributed to their delayed proliferation [1]. A greater understanding of these environments both in real-time and for ground testing yields the potential to define and improve the performance of the vehicle. The development of novel instrumentation that can withstand the extreme environment of HSVs whilst remaining capable of suitable characterization is of paramount importance. Optical instrumentation is uniquely suited for sensing in hypersonic environments owing to their robust and versatile properties. Fiber Bragg Gratings (FBGs) have been extensively employed for sensing applications and with a maximum operating temperature of 2050 °C for single crystalline sapphire optical fibers measuring hypersonic conditions is within reach [2, 3].

Typically, FBGs are permanently bonded to the outside of structures using cyanoacrylate or epoxy resins [4] and, in some cases, embedded inside composite structures [5]. For the case of wind tunnel testing where it is desired to reposition and reuse instrumentation to improve experiments and reduce cost, a permanent bonding method is undesirable. As an alternative, this work provides a preliminary examination upon the use of three different temporary adhesive tapes that would facilitate the reuse of FBGs.

1.1. Fiber Bragg Gratings

The development of suitable instrumentation capable of withstanding hypersonic environments is an important step towards the verification and understanding of such a flight regime. Optical instrumentation offers advantages over conventional electrical components including:

- high sensitivity,
- small size,

[1] *UNSW Canberra, 1 Northcott Drive, Campbell, ACT Australia, l.pollock@adfa.edu.au*
[2] *UNSW Canberra, 1 Northcott Drive, Campbell, ACT Australia, g.wild@adfa.edu.au*

- low weight,
- immunity to Electromagnetic Interference (EMI),
- low cost,
- versatile,
- and reliable [6].

Of the various forms of optical sensors, including interferometric and scattering, FBGs offer great potential in hypersonic applications due to their multiplexing capability and localized sensing. An FBG is an inline optical fiber sensor that functions as a wavelength specific filter. The grating is composed of a series of periodic dielectric mirrors with varying refractive index that is manufactured by inscribing a photosensitive optical fiber with an ultraviolet laser. The center reflected wavelength is known as the Bragg wavelength (λ_B) and can be deduced from the following relationship,

$$\lambda_B = 2n\Lambda \tag{1}$$

where n is the effective refractive index and Λ is the grating period. Several different grating patterns exist, including uniform, chirped, tilted, and phase shifted, all with unique applications.

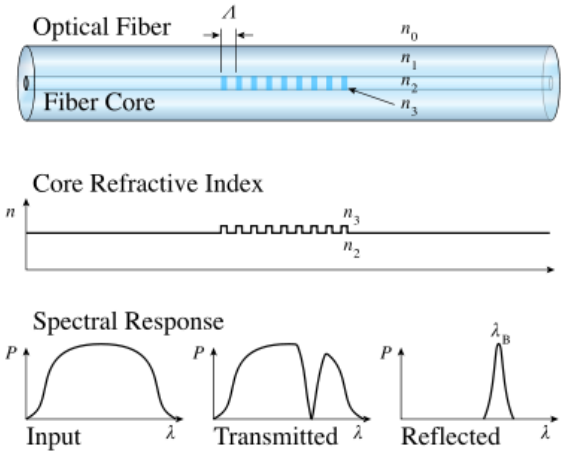

Fig 1. The fundamental principles of an FBG.

The response of the FBG to strain is governed by the theory of photoelasticity where the relative change in the Bragg wavelength is given by,

$$\frac{\Delta\lambda_B}{\lambda_B} = k_\epsilon \epsilon + k_T \Delta T \tag{2.1}$$

$$k_\epsilon = 1 - \frac{1}{2} n^2 [p_{12} - \nu(p_{12} + p_{11})] \tag{2.2}$$

$$k_T = \left[1 - \frac{1}{2} n^2 (p_{11} + 2p_{12})\right] \alpha + \frac{\xi}{n} \tag{2.3}$$

where ϵ is the mechanical strain, ΔT is the change in temperature, ν is the fibre Poisson's ratio, p_{11} and p_{12} are Pocknel's coefficients, α is the fibre coefficient of thermal expansion, and ξ is the fibre thermo-optic coefficient. As evident, an FBG is sensitive to both mechanical and thermal strain which typically requires isolating of one component, a variety of methods exist to accomplish this which generally employ FBGs in pairs. Alternative methods for strain isolation include birefringent [7] and chirped FBGs.

2. Methodology

2.1. Optical Setup

In this work an FBG was manually adhered to a rectangular aluminum panel of dimensions (1.65 x 60 x 150) mm. Tests were conducted with FBGs orientated longitudinally along the applied force axis as well as transverse to it. The FBG was illuminated through a circulator from a Thorlabs S5FC1005S Super Luminescent Diode (SLED) following which the reflected spectrum was measured using a Photonetics WALICS Optical Spectrum Analyzer (OSA). During testing a Shimadzu AG-X 50 kN Universal Testing Machine (UTM) was incrementally ramped from 0 N up to 2000 N in 100 N steps. A 60 second hold was applied at each step to allow for averaging of 32 samples. A depiction of the experimental setup is shown below in Fig 2.

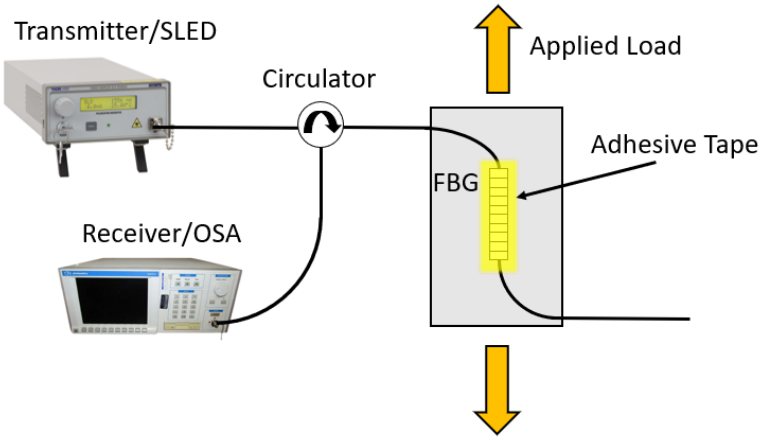

Fig 2. The optical experimental setup.

2.2. Temporary Adhesive Tapes

Three different tapes were assessed in this preliminary investigation. The first tape is a Japanese rice paper tape (Washi) coated with an acrylic adhesive that is typically used for masking of surfaces. The second tape is a fiberglass backed aluminum tape that is typically used in high-temperature environments, being specifically designed for application in automotive engines. The third and final tape tested is a double-sided tissue tape which is typically used in mounting applications. Photographs of the three tapes are shown in Fig 3 below.

a) b) c)

Fig 3. a) Washi tape, b) high-temperature tape, and c) double-sided tissue tape.

Ultimately, all three tapes offer unique benefits that must be considered in their selection. The Washi tape is very thin, easy to apply, semi-transparent, and offers good use up to a maximum of 100 °C. The high-temperature tape possesses a higher elastic modulus, increasing the efficiency of strain transfer whilst also being suitable for applications up to 400 °C. This tape whilst most suited for hypersonic testing is more expensive and opaquer, creating difficulty in correctly mounting the optical

instrumentation. Finally, the double-sided tape offers the likelihood of lowest strain transfer due to the adhesive being highly pressure sensitive but is transparent, making instrumentation easy to mount. The properties of all three tapes are summarized in Table 1 below.

Table 1. A summary of the tested tapes.

	Washi Tape	**High-Temperature Tape**	**Double-Sided Tape**
Adhesive	Acrylic	NA	Acrylic
Transparency	Semi	Opaque	Transparent
Relative Cost	Low	High	Moderate
Thickness (μm)	87	200	120
Max Temperature (°C)	100	400	80.0

2.3. Data Processing

Under an applied strain, the Bragg wavelength and spectra shifts according to the theory of photoelasticity given in Eq. 2.1 – 2.3. Following acquisition of the reflected spectra, a Generalized Cross-Correlation (GCC) was used to determine the wavelength shift. Due to the presence of side lobes and various spectrum fingers, the main peak lobe was isolated and used to determine the shift. Whilst straining of the fiber would result in small amounts of distortion such as narrowing of the bandwidth, the low forces used in testing render this distortion negligible. The GCC can be considered as a sliding dot product and is given below for a pair of discrete signals in the time domain, where $\overline{a_i[k]}$ represents the complex conjugate of signal $a_i[k]$.

$$\left(a_i \star a_j\right)[n] \triangleq \lim_{N\to\infty} \sum_{\lambda=-N}^{N} \overline{a_i[\lambda]} a_j[\Delta\lambda + \lambda] \tag{3}$$

The GCC can be more efficiently computed in the frequency domain using the Inverse Fast Fourier Transformation (IFFT) where $A_i(f)$ is the Fast Fourier Transformation (FFT) of $a_i[k]$.

$$\Delta\lambda = \max \mathbf{IFFT}\left|\overline{A_i[\lambda]} \cdot A_j[\lambda]\right| \tag{4}$$

The nature of GCC in a discrete domain permits only sample rate level accuracy, hence, a sub-sampling method is used to determine the wavelength shift. The Shape Language Modelling (SLM) toolbox in MATLAB was applied to ascertain an analogue for the continuous peak of the GCC function. Whilst this ultimately introduces a degree of uncertainty, the use of SLM permits the ability to undertaken analysis that would otherwise not be possible.

2.4. Uncertainty Analysis

The uncertainty surrounding the applied instrumentation and data processing techniques yields a requirement to understand the effects of error. As such, a linear uncertainty analysis has been applied to quantify the propagation of uncertainty. In this work, thermal strain is assumed to be negligible and as such, the shift in Bragg wavelength is given by Eq. 5.

$$\Delta\lambda_B = \varepsilon\lambda_\mathrm{B}\left(1 - \frac{1}{2}n^2[p_{12} - \nu(p_{12} + p_{11})]\right) \tag{5}$$

From Eq. 5, the differential of $\Delta\lambda_B$ can then be calculated as follows.

$$d\Delta\lambda_B = \left(\frac{\delta\Delta\lambda_B}{\delta\varepsilon}\right)\Delta\varepsilon + \left(\frac{\delta\Delta\lambda_B}{\delta\lambda_B}\right)\Delta\lambda_B + \left(\frac{\delta\Delta\lambda_B}{\delta n_\mathrm{eff}}\right)\Delta n + \left(\frac{\delta\Delta\lambda_B}{\delta\nu}\right)\Delta\nu + \left(\frac{\delta\Delta\lambda_B}{\delta p_{12}}\right)\Delta p_{12} + \left(\frac{\delta\Delta\lambda_B}{\delta p_{11}}\right)\Delta p_{11} \tag{6}$$

The full list of partial derivatives in provided in Appendix A. Centre values and confidence intervals are obtained from Bertholds and Dandliker [8] and Wang, et al. [9]. The central value component is taken as the idealized Bragg wavelength shift and can then be used to also calculate the strain efficiency of each adhesive tape (how much strain is transferred to the fiber). A summary of fiber parameters is given in Table 2 below.

Table 2. Summarised optical fibre parameters.

Parameter	Centre Value	Error (±)
$\boldsymbol{\nu}$	0.154	0.018
$\boldsymbol{p_{11}}$	0.113	0.005
$\boldsymbol{p_{12}}$	0.252	0.005
$\boldsymbol{\lambda_B}$ (nm)	1556.54	0.01
$\boldsymbol{n}$	1.458	0.0729

3. Results and Discussion

Measurement uncertainty has been obtained from the manufacturer's technical datasheets. The Shimadzu UTM possesses a force accuracy of ±0.5 % beyond 0.2 % of the maximum load cell rating (100 N). Force values below 100 N have been marked, as seen in Fig 4, as a region of high uncertainty of which the manufacturer does not provide accuracy specifications. Likewise, displacement is measured using an embedded optical encoder which specifies an accuracy of ±0.1 % or ±0.01 mm. In this case, displacements are small enough such that ±0.01 mm is taken as a constant error for all data points. Finally, the Photonetix WALICS specifies a wavelength accuracy of ±40 pm, a relatively large degree of uncertainty that from the results, appears to be very conservative. Future experiments aim to employ extensometers to reduce the strain uncertainty whilst testing above 250 N would avoid the region of high uncertainty.

3.1. Raw Data

Figure 4 below shows time-stress, time-strain, and stress-strain curves derived from the UTM. Each of the data collection points, marked by a red cross, also indicate the relative uncertainties in measurements as obtained by the manufacture's specifications. The highlighted red region is of high uncertainty as it is less than the 100 N specified. It can be clearly observed that in the stress-strain curve that an inflection point occurs at approximately 1000 με, highlighting the lack of confidence in the data collected below this region. Above 1300 με, the curve becomes relatively linear as would be expected. In future experiments, additional instrumentation should be utilized to reduce uncertainty in the data.

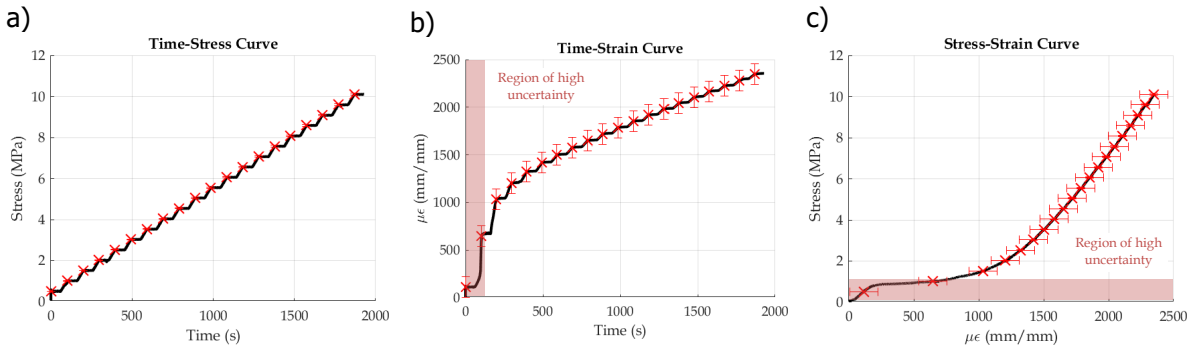

Fig 4. Sample data acquired from the UTM showing the a) time-stress, b) time-strain, and c) stress-strain curves.

Figure 5 below provides a sample of the acquired logarithmic reflected spectrum from the OSA. This figure, at zero strain, indicates a Bragg wavelength of 1556.54 nm that is marked by the red cross. The central region likewise corresponds to the truncated portion of the spectrum that has been used to complete the GCC and estimate the wavelength shift. Whilst the wavelength shift could be estimated by the difference in Bragg wavelength, it can be observed that the top of the spectrum is relatively flat that could result in errors if this approach was used.

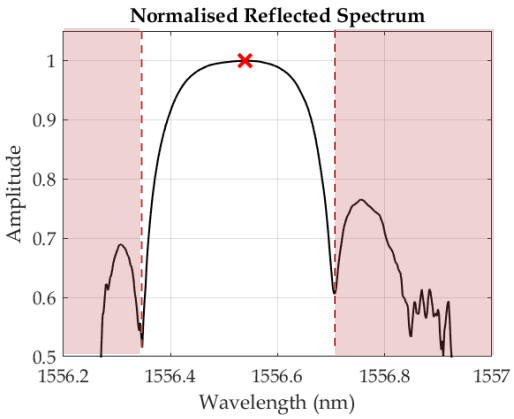

Fig 5. Sample data acquired from the OSA.

3.2. Processed Data

Post-processing of the raw data is completed by firstly completing a linear regression with the strain as the abscissa and wavelength shift as the ordinate values, respectively. Results for longitudinal testing and transverse testing are shown in Fig 6 and Fig 7, respectively. Linear regression results are summarized in Table 3.

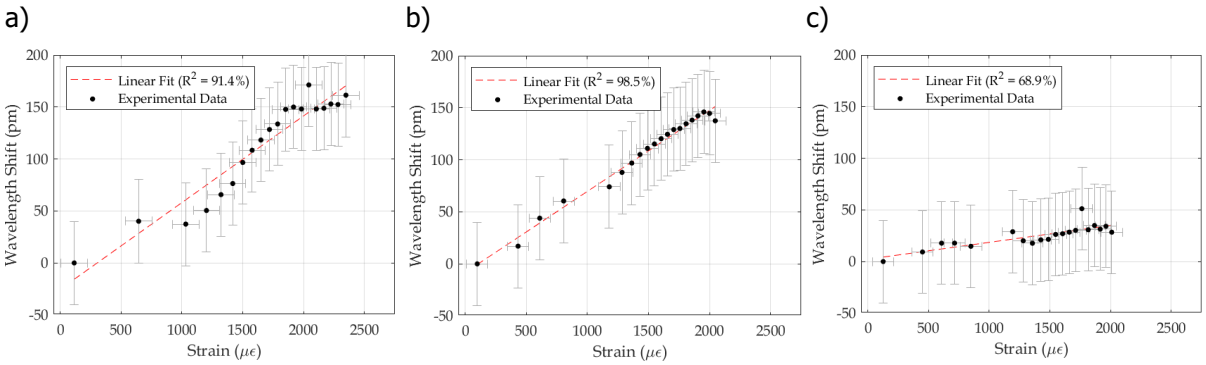

Fig 6. Linear regression fits under longitudinal testing for a) Washi, b) high temperature, and c) double-sided tape.

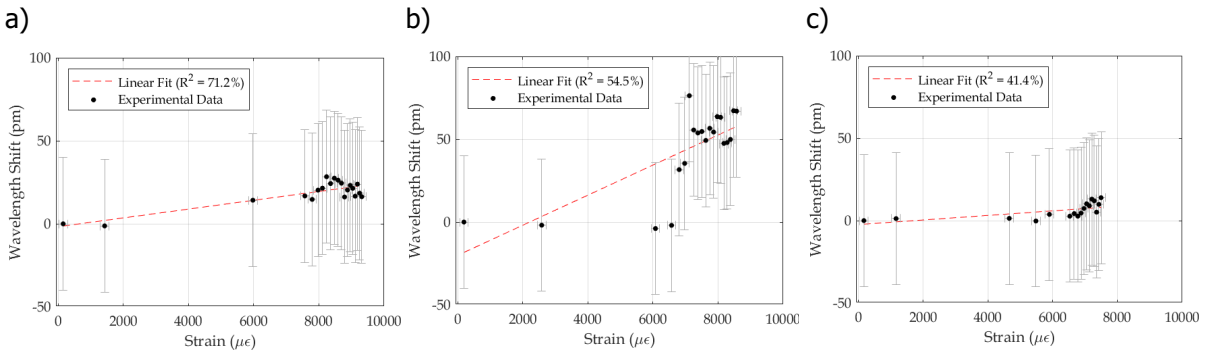

Fig 7. Linear regression fits under transverse testing for a) Washi, b) high temperature, and c) double-sided tape.

Table 3. Summarised regression properties for both the longitudinal and transverse testing.

	Longitudinal			Transverse		
Tape	Linearity (R^2)	RSME	Sensitivity (pm/με)	Linearity (R^2)	RSME	Sensitivity (pm/με)
Washi	91.4 %	15.09	0.0834	71.2 %	4.314	0.0027
High Temp	98.5 %	5.364	0.0780	54.5 %	17.59	0.0091
Double-Sided	68.9 %	6.155	0.0163	41.4 %	3.661	0.0014

For longitudinal test, the Washi tape showcased the greatest sensitivity at 0.0834 pm/με whilst the high temperature tape revealed the greatest linearity with a Coefficient of Determination (CoD) of 98.5 %. The double-sided tape offers both the lowest sensitivity and linearity. Whilst the Washi and high temperature tape sandwich the sensor between the test coupon, the double-sided tape exposes the sensor to the external environment which improves the likelihood of slippage and decreases strain transfer. Hence, whilst the double-sided tape is the easiest to apply and in which the sensor can be most accurately placed it is not suitable for adhering FBGs.

For transverse testing, there is no applied load along the sensor axis, therefore any strain induced would be the result of contraction from the Poisson's effect and should reflect a compressive force. However, it was observed that the wavelength shift indicated a tensile strain, therefore there is a high likelihood that the observed wavelength shift resulted from misalignment of the sensor along the transverse axis. Despite this, the high temperature tape presented with the greatest sensitivity at 0.0091 pm/με whilst the Washi was the most linear with a CoD of 71.2 %.

3.3. Strain Efficiency

A useful metric in quantifying the efficacy of each adhesive tape is strain efficiency. The strain efficiency is given as the observed strain as a percentage of the ideal strain. By applying Eq. 5, a linear relationship can be deduced for the specific FBG utilized. Furthermore, to account for the presence of measurement uncertainty, the linear propagation of uncertainty relationship, deduced from Eq. 6, has been applied to estimate the upper and lower confidence bounds. The resulting relationship, shown in Fig 8 a), allows for determination of the idealized wavelength shift under an applied strain, accounting for uncertainty. Figure 8 b) similarly showcases the relationship between wavelength shift uncertainty and strain uncertainty for a variety of ideal strain values.

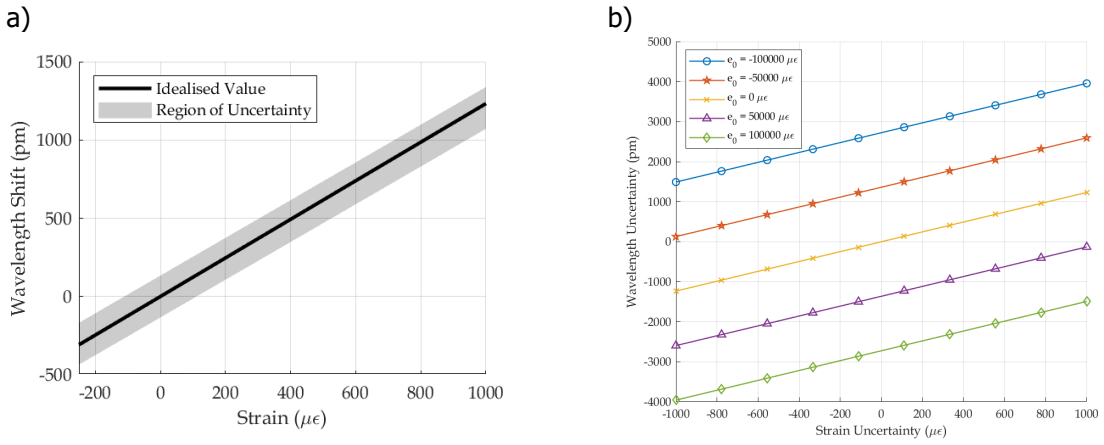

Fig 8. a) Wavelength shift versus strain, accounting for uncertainty and b) wavelength uncertainty versus strain uncertainty for several ideal strain values.

Application of the deduced relationship for centrally located idealized wavelength shift results in Fig 9 for each of the adhesive tapes. From this, it is evident that the high temperature tape offers the greatest strain efficiency with a median longitudinal and transverse efficiency of 6.04 % and 1.70 %, respectively. The presence of outliers is also noted and is marked with a black cross.

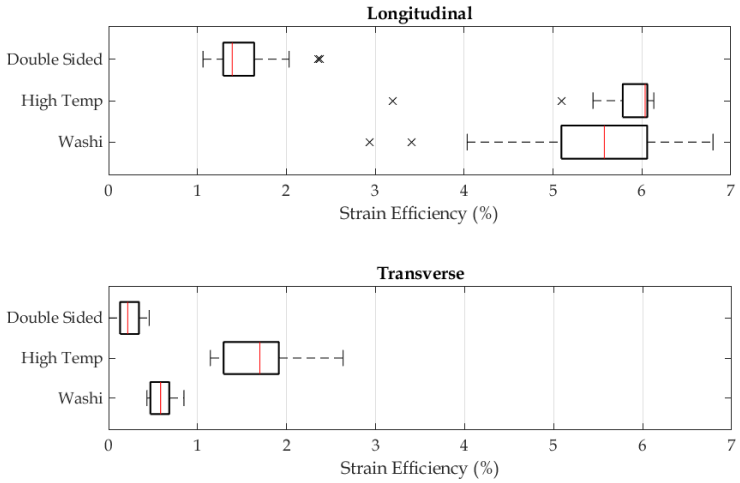

Fig 9. Strain efficiencies for each of the adhesive tapes under longitudinal and transverse loading.

A comparison of strain efficiencies achieved when adhering FBGs with cyanoacrylates, acrylic, and epoxy resins is shown in Table 4. The permanent adhesives clearly reveal superior strain transfer, as expected, but do not allow for repositioning or reuse of equipment.

Table 4. A comparison of strain efficiencies between temporary and permanent adhesives.

	Longitudinal Strain Efficiency			**Transverse Strain Efficiency**		
Tape	Median	Maximum	Minimum	Median	Maximum	Minimum
Washi	5.577 %	6.799 %	4.034 %	0.5844 %	0.8468 %	0 %
High Temp	6.036 %	6.134 %	5.449 %	1.670 %	2.635 %	0 %
Double Sided	1.391 %	2.379 %	1.062 %	0.2158 %	0.4559 %	0 %
Adhesive						
Epoxy **[10]**	99.20 %	NA	NA	NA	NA	NA
AB (Polyurethane) **[10]**	93.80 %	NA	NA	NA	NA	NA
502 (Cyanoacrylate) **[10]**	96.50 %	NA	NA	NA	NA	NA

4. Conclusion

Whilst adhesive tapes have proved suitable for the bonding of FBGs to substrate material, they greatly suffer from poor strain efficiencies, thereby reducing sensitivity and accuracy of the sensor system. However, the use of such temporary adhesives allows for the reuse and repositioning of equipment in prototyping and their application should not be disregarded. From this preliminary investigation, both the Washi and high temperature tapes prove to be the most suitable, offering the best linearity and sensitivity. The Washi tape – being semi-transparent – allows for more accurate positioning of the sensor on the substrate whilst the high temperature tape is more suitable for demanding thermal and mechanical environments. The authors plan to expand this study to encompass a greater variety of temporary adhesives – including putties and thermoplastics – as well as to develop a more repeatable and efficient methodology. Future testing will also be expanded to account for compressive, bending, and multi-axial loading as well as thermal effects.

References

1. L. Pollock and G. Wild, An initial review of hypersonic vehicle accidents, in 19th Australian International Aerospace Congress, Melbourne, Australia, 2021.
2. T. Habisreuther, T. Elsmann, Z. Pan, A. Graf, R. Willsch, and M. A. Schmidt, Sapphire fiber Bragg gratings for high temperature and dynamic temperature diagnostics, Applied Thermal Engineering, vol. 91, pp. 860-865, 2015.
3. L. Pollock and G. Wild, Modal Analysis of a Scramjet Inlet for Optimization of Sensor Placement, in ASCEND 2021, 2021: American Institute of Aeronautics and Astronautics, in ASCEND, doi: doi:10.2514/6.2021-4084.
4. P. Motwani, N. Perogamvros, S. Taylor, M. Sonebi, A. Laskar, and A. Murphy, Experimental investigation of strain sensitivity for surface bonded fibre optic sensors, Sensors and Actuators A: Physical, vol. 303, p. 111833, 2020.
5. L. Jin *et al.*, An embedded FBG sensor for simultaneous measurement of stress and temperature, IEEE Photonics Technology Letters, vol. 18, no. 1, pp. 154-156, 2005.
6. G. Wild and S. Hinckley, Acousto-ultrasonic optical fiber sensors: Overview and state-of-the-art, IEEE Sensors journal, vol. 8, no. 7, pp. 1184-1193, 2008.
7. E. Lindner *et al.*, Trends and future of fiber Bragg grating sensing technologies: tailored draw tower gratings (DTGs), in Optical Sensing and Detection III, 2014, vol. 9141: International Society for Optics and Photonics, p. 91410X.
8. A. Bertholds and R. Dandliker, Determination of the individual strain-optic coefficients in single-mode optical fibres, Journal of lightwave technology, vol. 6, no. 1, pp. 17-20, 1988.
9. P. Wang, G. Farrell, Q. Wang, and G. Rajan, An optimized macrobending-fiber-based edge filter, IEEE Photonics Technology Letters, vol. 19, no. 15, pp. 1136-1138, 2007.
10. H. Tian, D.-g. Liu, Y.-p. Wang, and Q.-l. Wang, Effect of adhesive type on the sensitivity coefficient of FBG sensor bonded on the surface of CFRP, Optoelectronics Letters, vol. 15, no. 4, pp. 264-268, 2019.

Appendix A

$$\left(\frac{\delta\Delta\lambda_B}{\delta\varepsilon}\right) = \lambda_B\left(1-\frac{1}{2}n_{\text{eff}}^2[p_{12}-\nu(p_{12}+p_{11})]\right)$$

$$\left(\frac{\delta\Delta\lambda_B}{\delta\lambda_B}\right) = \varepsilon\left(1-\frac{1}{2}n_{\text{eff}}^2[p_{12}-\nu(p_{12}+p_{11})]\right)$$

$$\left(\frac{\delta\Delta\lambda_B}{\delta n_{eff}}\right) = -\varepsilon\lambda_B n[p_{12}-\nu(p_{12}+p_{11})]$$

$$\left(\frac{\delta\Delta\lambda_B}{\delta\nu}\right) = \frac{1}{2}n^2\varepsilon\lambda_B(p_{12}+p_{11})$$

$$\left(\frac{\delta\Delta\lambda_B}{\delta p_{12}}\right) = \frac{1}{2}\varepsilon\lambda_B n^2(\nu-1)$$

$$\left(\frac{\delta\Delta\lambda_B}{\delta p_{11}}\right) = \frac{1}{2}\varepsilon\lambda_B n^2\nu$$